A study of side-chain ordering in oriented rigid-rod polyesters

Ladislav Červinka
Institute of Physics, Academy of Sciences of the Czech Republic, 162 00 Praha 6, Czech Republic
(Received 28 May 1992; revised 23 August 1993)

It is shown that the structure of biaxially oriented polyester poly(1,4-phenylene-2,5-di-*n*-alkoxyterephthalate), with the length of the *n*-alkoxy side chains being $n=16$, can be interpreted as a mixture of incommensurate structures. The principal one describes the ordering of rigid rods using an orthorhombic cell. The structure of side chains in a quickly stretched film is described by a monoclinic and a triclinic cell. An orthorhombic cell helps to describe the slowly stretched film. The monoclinic cell was found on the basis of our model calculations of X-ray scattering on a powder sample of this polyester, documenting that there is a clustering of side chains. Further, the ordering of side chains in the amorphous phase anticipates the interchain distance characteristic for the crystalline-like arrangements of side chains in the biaxially oriented films, because the average distance between side chains calculated from all incommensurate structures is 4.8 Å, i.e. precisely the distance found between clustered side chains in the amorphous phase.

(Keywords: polyester; side-chain ordering; rigid-rod structure)

INTRODUCTION

General

The aim of this paper is to point out the connection between the amorphous structure of side chains in rigid-rod polyesters and structures that we have found in oriented (stretched) polyesters.

First, however, we review two important results of a paper[1] in which we have studied the structure of a polyester, poly(1,4-phenylene-2,5-di-*n*-alkoxyterephthalate), with the length of *n*-alkoxy side chains being $n=16$

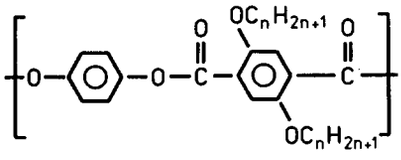

(PPT16). Without knowledge of these results it would be impossible to understand fully the structural relations in this class of oriented and unoriented polyesters. The structural analysis of this polyester (consisting of rigid rods and flexible side chains) was done on the basis of an X-ray scattering picture (*Figure 1*) taken on its powder sample prepared by melting to approximately 150°C and then quenching to room temperature[2].

The main problem with this material and its X-ray scattering picture was the analysis of the complex overlapping peaks at 1.46 and 1.75 $Å^{-1}$, which evidently had (in contrast to massive peaks at 0.25, 0.50 and 0.75 $Å^{-1}$) a non-crystalline character. The method of analysis consisted, as in our previous work[3,4], of a direct calculation of the X-ray diagram by the Debye formula using different structural models. The Debye equation gives the dependence of the average scattered intensity $I(s)$ for an array of atoms or identical objects, with a completely random orientation in space, on the angle θ and on the wavelength λ:

$$I(s)=\sum\sum f_i f_j(\sin sr_{ij})/sr_{ij} \quad (1)$$

where f_i, f_j are the X-ray scattering factors, s is the scattering vector in the reciprocal space and r_{ij} are the distances between atoms.

It is important to note that in order for a crystalline powder sample to simulate a classic Debye–Scherrer powder pattern it is necessary to calculate with more than 10^4 atoms, i.e. with the number of adjacent elementary cells being of the order $>10^1$. Only then are we able to calculate signals from lattice planes of low occupancy in powder samples of crystalline structures characterized by lower symmetries. In a non-crystalline material, however, the criterion of long-range order periodicity (i.e. of periodicity extending over one elementary cell) is not valid, hence the requirements on the number of atoms necessary for the calculation of medium-range order-dependent features of the X-ray diagram are not so exacting. In other words: a calculation of X-ray scattering using the Debye formula for a number of atoms which is smaller than the number of atoms in an elementary cell defining a crystalline structure, results in an X-ray scattering picture typical of non-crystalline materials.

Clustering of side chains

Figure 1 reviews the result of our calculation of X-ray scattering for the above-cited polyester[1]. The calculation is based on a model of ordering of rigid rods with side chains shown schematically in *Figure 2*. It consists of six layers ($6\times312=1872$ atoms); in every layer there are two rigid rods ($2\times54=108$ atoms) and 12 side chains ($12\times17=204$ atoms).

The basic result of our previous work was that in order to obtain the correct position of the liquid-like (non-crystalline) peak at 1.46 $Å^{-1}$ in the X-ray scattering

0032-3861/94/24/5225–10

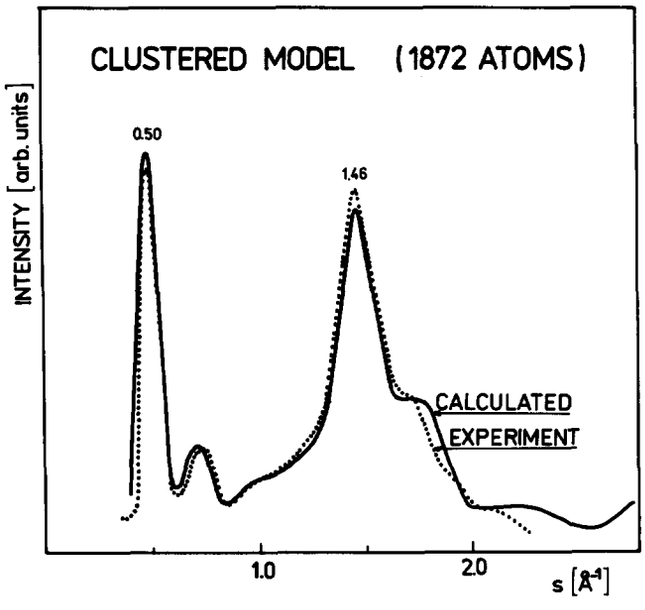

Figure 1 Comparison of experimental (···) and calculated (——) X-ray scattering on the basis of the model of clustered side chains as shown in *Figure 3*; see text for details

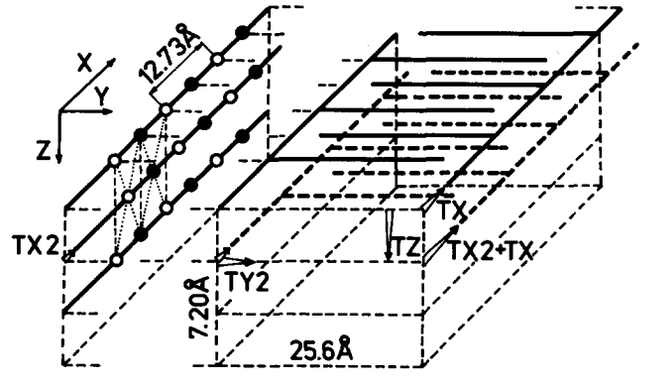

Figure 2 Generation of the model for a polyester with rigid rods and flexible side chains. The model consists of six *x,y* layers. Rigid rods are oriented in the *X* direction. Parameters *TX*, *TZ* and *TX2* enabled the study of various shifts of rigid rods ($TX = 3.60$ Å). The *TY2* parameter which introduces a disorder of rigid rods out of *X,Z* planes is important. In the *X,Z* projection of the structure, side chains are shown by open circles; however, 'intercalated' side chains, having their origin in the neighbouring rigid rod, are shown as solid circles

diagram we have to propose a structural model (*Figure 3*) which consists of clustering of side chains.

Let us explain what we understand by clustering. Clustering means that the average distance between clustered side chains in a certain volume is smaller than it would be when determined only by the repeating unit of the main rigid rod. We showed in a previous paper that the distance between side chains that were attached to a single rigid rod was 10.984 Å, while the repeating distance of the rigid rod was 12.734 Å. Such a model of side-chain clustering is shown in *Figure 3* in a projection into the *X,Y* plane. Denser packing of side chains is achieved by a non-zero value of the clustering parameter *TQ*. This parameter measures the shift of the first and third side chains towards the second one, as indicated in *Figure 3*. It is clear that the locus of the first side-chain CH_2 group is fixed by the position along the main chain. Thus only parts of the side chains having a sufficient distance to the main chain can take part in the clustering process. We have supposed, however, that this idealized model (thin full lines) could serve as a reasonable approximation of real ordering of side chains (thick full lines).

We also wish to emphasize an important quantitative result of our calculations concerning the magnitude of the area in which the clustering takes place. The analysis presented in ref. 1 showed that a regular ordering of clustered side chains must be realized in a region at least $40 \times 52 \times 20 \approx 4 \times 10^4$ Å^3 (with a total of about 1900 atoms simultaneously in rigid rods and flexible side chains). Only under this condition was it possible to explain the relatively intense peak at 1.46 Å^{-1} (see *Figure 1*).

The crystalline interpretation of unoriented polyester samples

Before starting to study scattering diagrams of oriented polyesters, we should review a second important result of our previous work[1].

We have demonstrated (*Figure 4*) that it is also possible to simulate the experimental X-ray scattering diagram of the powder polyester sample on the basis of crystalline elementary cells. This result may help us later on to find the computational transition (i.e. the crystallographic parameters) for the solution in the single-crystal

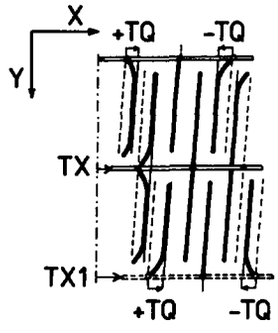

Figure 3 Generation of clustered side chains in the *X,Y* plane of the computer model. The original position of side chains is visualized by a dashed line; the idealized position of clustered side chains used in the calculation is shown by a full thin line. The clustering parameter *TQ* describes the shift of the side chains from their original position and has a value of 1.75 Å. Parameters *TX* and *TX1* enable a shift of rigid rods in the *X* direction in order to obtain a regular arrangement of clustered side chains. Thick lines model the supposed real ordering of side chains

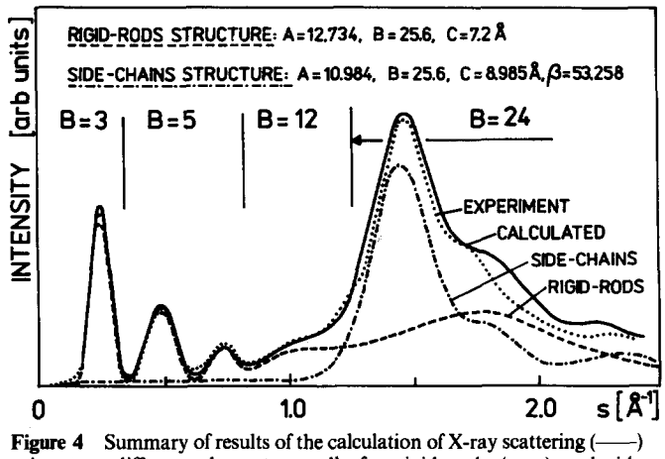

Figure 4 Summary of results of the calculation of X-ray scattering (——) using two different elementary cells for rigid rods (– – –) and side chains (–·–·–). Values of the Gaussian broadening coefficient *B* correspond only to the calculation of the rigid-rod contribution in the given interval (see text for details)

approximation. Two different cells are used: an orthorhombic one describes the ordering of rigid rods ($A = 12.734$ Å, $B = 25.6$ Å and $C = 7.2$ Å), and a monoclinic elementary cell ($a_m = A = 10.984$ Å, $B = 25.6$ Å, $c_m = C = 8.985$ Å and $\beta = 53.258°$) is used for the calculation of X-ray scattering dependent on the ordering of side chains (see also later).

In order to understand the calculation shown in *Figure 4*, it should be borne in mind that this includes a calculation of about 560 structure factors, F^2_{hkl}, for both structures, then a convolution of these sets of structure factors by different Gaussian broadening functions (the width of the Gaussian broadening function is characterized by the B parameter) dependent on the s parameter. Generally, the greater the s parameter the broader is the corresponding Gaussian broadening function. For the monoclinic structure of side chains we use relatively broad broadening functions (the parameter B characterizing the broadening of a Gaussian distribution has a value of 12 for structure factors in the intervals $s < 2$ Å^{-1}, and 24 in the interval $2 < s < 2.5$ Å^{-1}).

The main conclusion from the above calculation is that the monoclinic cell parameter describing the ordering of side chains in the X-direction has a value $A = 10.984$ Å. This value confirms that the distance between side chains has to be smaller in the X-direction than the repeating distance of the rigid rod, i.e. 12.74 Å. This is another strong argument in favour of the clustering model describing the ordering of side chains.

Further, the necessity to use relatively broad modifying Gaussian functions for the simulation of the X-ray scattering diagram documents the non-crystalline character of the side-chain ordering calculated on the basis of a crystalline lattice cell.

Oriented polyesters

While we were studying the structure of polycrystalline polyesters, a dissertation[5] appeared on phase and structural relations in oriented samples of polyesters having the same composition. Hence the important question arose of whether the concept of clustered side chains is also able to explain the main features of X-ray diagrams taken on oriented polyesters, because only if this is the case may this concept be considered to be self-consistent. We shall show in this paper that the answer to this question is definitely positive.

CALCULATION OF X-RAY DIAGRAMS OF ORIENTED SAMPLES

Experimental

Figure 5 summarizes X-ray diagrams[5] of quickly and slowly stretched PPT16 films prepared at 40°C and at room temperature, taken with the incident X-ray beam perpendicular and parallel to the plane of the film. The lattice distances ascribed in *Figure 5* to the most intensive reflections in ref. 5 have only informative character, because according to their width, the lattice distance d may vary in the limits $d = \pm 0.15$ Å. We shall abbreviate the expression 'X-ray diagram taken with an incident X-ray beam perpendicular/parallel to the plane of the PPT16 film' as 'a perpendicular/parallel X-ray diagram'.

The most important key for the understanding and interpretation of X-ray diagrams of biaxially stretched PPT films is to have a correct relation between the model of the structure and the macroscopic shape of the film.

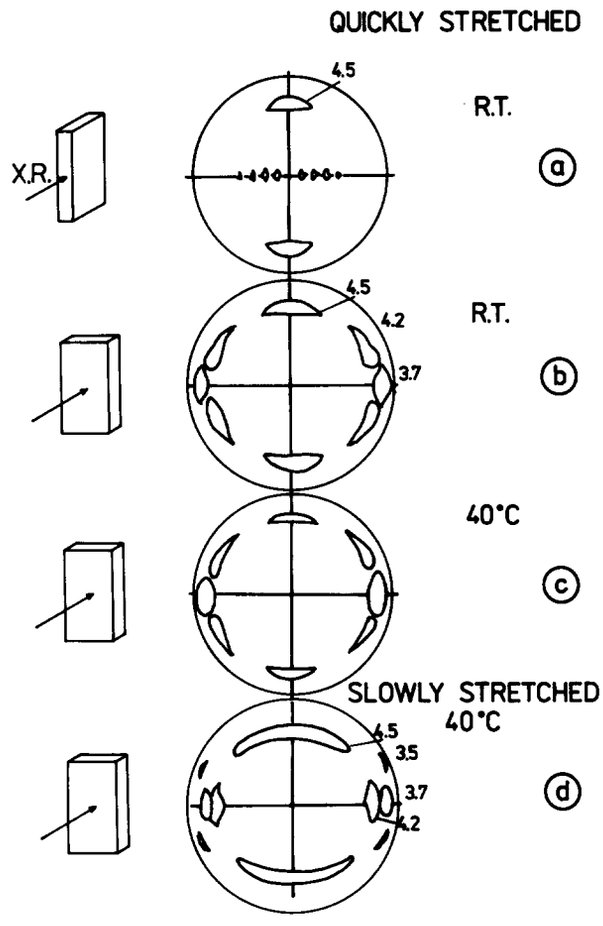

Figure 5 X-ray diagrams of quickly and slowly stretched PPT16 films[5] prepared at room temperature (incident X-ray beam perpendicular and parallel to the plane of the film) and at 40°C (incident X-ray beam perpendicular to the plane of the film). Only the most intense reflections are visualized, see text for comment. Numbers denote lattice distances (in Å) ascribed in ref. 5 to these reflections

This relation is schematically visualized in *Figure 6*. The basic information is that in our notation the plane of the film is identical with the X,Z plane of the model.

Calculation on the basis of the rigid-rod structure

The main problem with the analysis of the oriented samples lies in the question, 'to what extent is the model that explains the structural behaviour of the unoriented (powder) samples able to describe at the same time the structure of oriented films?' In other words, what modifications, if any, of the present model are necessary in order to obtain the observed X-ray patterns of the oriented film? We shall therefore proceed with a calculation of X-ray diagrams of biaxially oriented films for the model proposed in *Figure 4*. The model proposed for rigid rods is based on an orthorhombic elementary cell with lattice parameters:

$$A = 12.734 \text{ Å}; \; B = 25.6 \text{ Å}; \; C = 7.2 \text{ Å} \qquad (2)$$

The calculation of structure factors in *Figure 7* enabled us to obtain a distribution of intensity in the reciprocal space. It follows from *Figure 6* that the film is stretched, in our notation, in the direction of the X axis, i.e. the X-ray beam is perpendicular to the rigid-rod axis X. Hence the intensity distribution in the X-ray diagram must be a consequence of the intensity distribution in

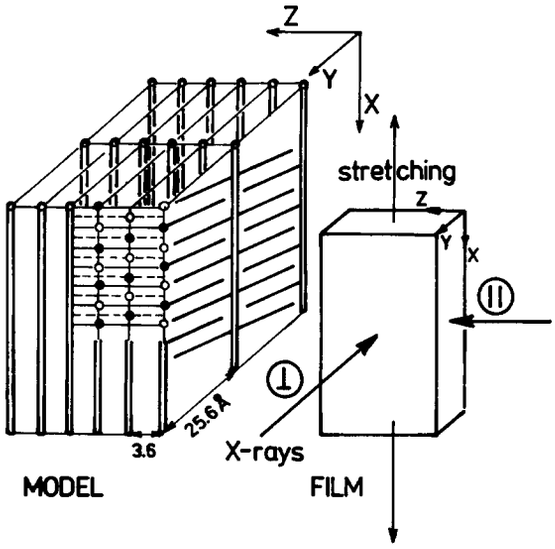

Figure 6 Relation between the macroscopic shape of a PPT16 film and the orientation of our structural model describing ordering of rigid rods with side chains. Compare this figure with *Figure 2*

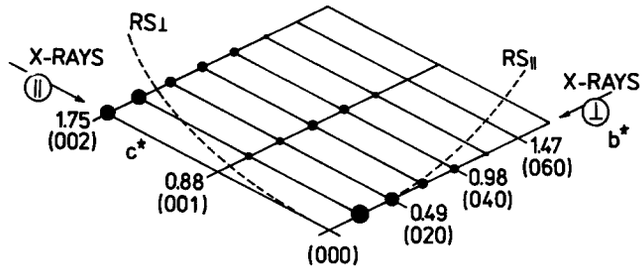

Figure 7 Example of the calculation of structure factors F^2 in a section of a reciprocal lattice layer (0,b^*,c^*) corresponding to the orthorhombic structure of rigid rods. Values of structure factors $F^2 > 1000$ are visualized by solid circles having a corresponding diameter. Values on the axis denote absolute values of the reciprocal lattice vectors (in $Å^{-1}$) and their (*hkl*) indices. Only a section of the reciprocal lattice extending to $2\,Å^{-1}$ is shown, because only this one is documented in the corresponding X-ray diagram. The direction of the incident X-ray beam perpendicular to the film surface and the corresponding reflection spheres (RS) are shown (---)

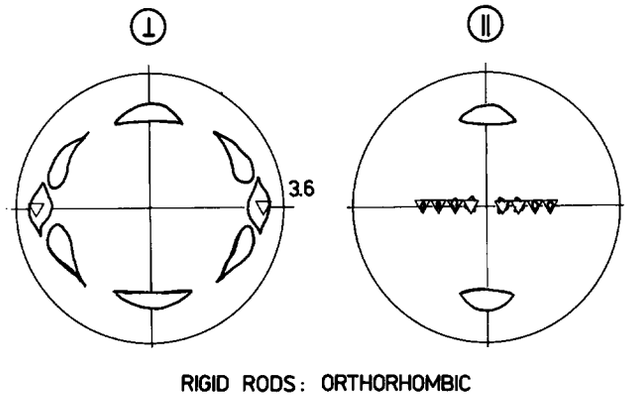

Figure 8 Superposition of the experimental with the calculated X-ray diagram corresponding to the intensity distribution shown in *Figure 7* for an X-ray beam perpendicular and parallel to the film surface. The contours of the experimental X-ray diagrams are shown by thick lines. The value of 3.6 Å is the corresponding lattice distance in the perpendicular case. In the parallel X-ray diagram, the values corresponding to the equatorial reflections are 25.6, 12.8, 8.5 and 6.4 Å

reciprocal b^*, c^* planes. The intensity distribution in the 0,b^*,c^* plane is demonstrated in *Figure 7*; further layers are not significant, because calculated intensities in these layers were smaller than 1000.

The construction of X-ray diagrams is then a consequence of conditions during which the given reflection sphere intersects reciprocal lattice points; this procedure is then followed by an appropriate stereographic projection. The reflecting sphere cuts and/or nearly touches the most intensive reciprocal lattice points (located on the b^* axis) only when the direction of the X-ray beam is identical with the c^* axis. This situation corresponds to the case when the incident X-ray beam is parallel to the film surface (compare with *Figure 6*).

Figure 8 shows the superposition of the calculated with the experimental X-ray diagram. Rigid rods express themselves on the parallel X-ray diagram (i.e. X-rays in the direction of the c^* axis) as a set of equatorial reflections (0k0) characterized by lattice distances 25.6, 12.8, 8.5 and 6.4 Å (marked by triangles in *Figure 8*). This result agrees well with the observed X-ray diagram in *Figure 5a*. The perpendicular X-ray diagram contributes the structure of rigid rods only as an equatorial reflection (002) characterized by the lattice distance 3.6 Å, see the reflection marked 3.7 in *Figure 5b*.

Calculation on the basis of side-chain ordering

Calculation based on a monoclinic elementary cell. *Figure 4* represents our proposal of how to describe side-chain ordering by a monoclinic elementary cell. In order to have a more profound look into the structural relations of side chains, *Figure 9* shows a projection of side chains into the X,Z plane and we visualize the monoclinic cell:

$$a_m = A = 10.984\ Å;\ b_m = B = 25.6\ Å;\ C = c_m = 8.98\ Å;$$
$$\beta = 53.3° \qquad (3)$$

The repeating unit of the rigid rod is 12.734 Å long and the value of the clustering parameter TQ (see *Figure 3*) is 1.75 Å, hence $12.734\ Å - TQ = 10.984\ Å = a_m = A$.

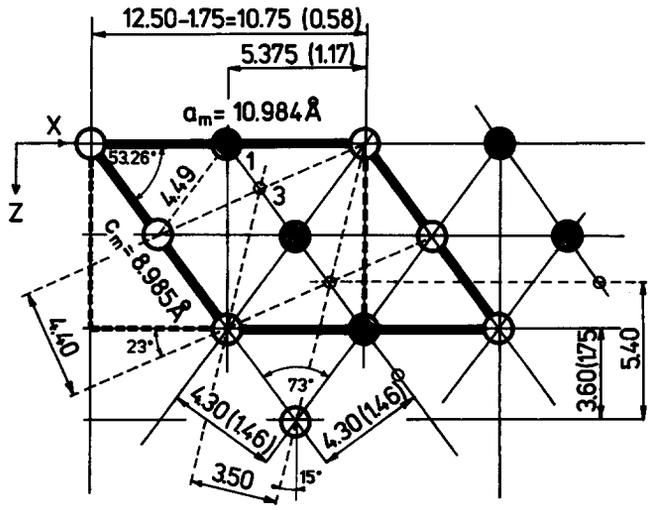

Figure 9 Projection of clustered side chains into the X,Z plane (compare with *Figure 2*). The monoclinic elementary cell (parameters a_m, c_m) is visualized by thick solid lines. Distances between 'lattice planes' are given in Å; numbers in brackets are the corresponding s values in $Å^{-1}$

However, the distance between non-clustered and clustered side chains is 12.50 and 10.75 Å, respectively. The difference between the monoclinic lattice parameter $A = 10.984$ Å and the distance 10.75 Å between clustered side chains in the X,Y plane is caused by the fact that side chains are not perpendicular to the rigid-rod axis X.

In this monoclinic cell the angle β is defined as the angle between positive directions of the model X and Z axis. Hence the angle β is not obtuse as it should be for a conventional monoclinic cell. Supposing that $\beta = 126.7°$, the results and conclusions following from our calculations based on this obtuse β angle would be identical with those already presented. The only difference would be in the indexing of reciprocal lattice points. This is also the reason for the definition of this monoclinic cell using:

$$A = 10.984 \text{ Å}; \; B = 25.6 \text{ Å}; \; C = 8.98 \text{ Å}; \; \beta = 126.7° \quad (4)$$

Now we proceed consistently as in the case of the rigid-rod structure (*Figures 7* and *8*). In *Figure 10* the X-ray diagram is calculated for the arrangement of side chains described by the monoclinic cell, see equation (4). *Figure 10a* presents larger sections of the reciprocal space in the case when intercalated side chains are located in position 1 (see *Figure 9*). This situation is characterized

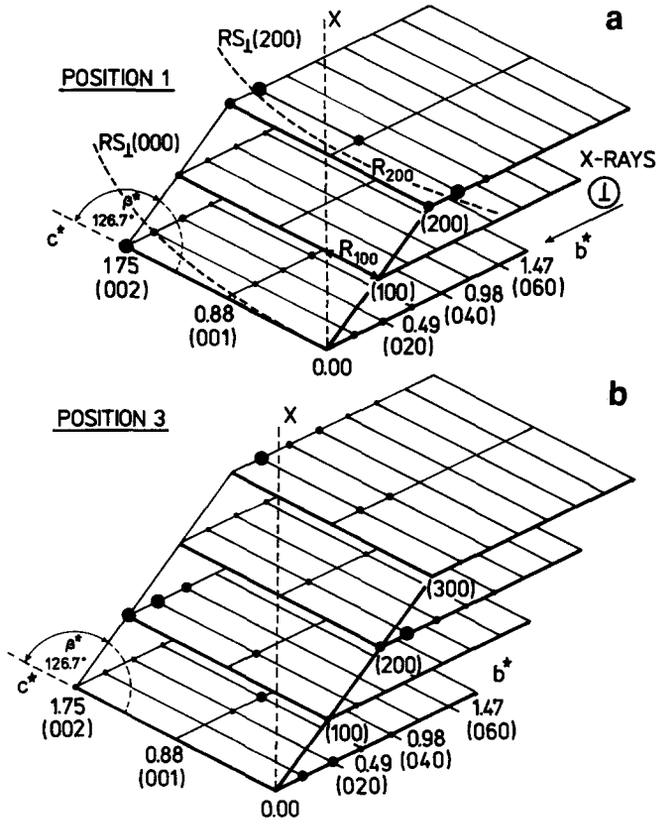

Figure 10 Reciprocal lattice of side chains described by the monoclinic cell, equation (4). Reciprocal lattice layers of the sequence [0,b*,c*], [1,b*,c*], [2,b*,c*] and [3,b*,c*] are shown; they are perpendicular to the rigid-rod axis X. (a) The intensity distribution when intercalated side chains were in position 1 (according to *Figure 9*). The third plane is omitted because there is no remarkable intensity distribution. The position of reflection spheres RS⊥(000) and RS⊥(200) for the zero and second layer are shown only for the perpendicular X-ray diagram. The numbers close to the b* and c* axis are values of the s-parameter for the given (0k0) and (00l) points. (b) Intensity distribution in the reciprocal space when intercalated chains are in position 3. It is important to note that in both cases the X axis lies in the [a*,0,c*] plane

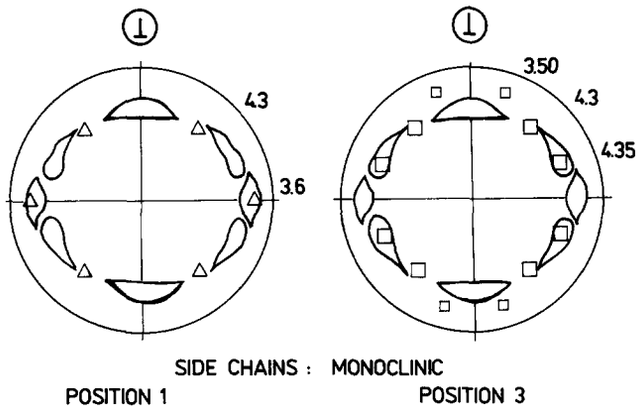

Figure 11 Superposition of the experimental and calculated perpendicular X-ray diagram (the contribution of these structures to the parallel X-ray diagram is zero). Numbers denote calculated lattice distances in Å. Contours of the experimental X-ray diagram are shown by a thick line. Left, intercalated side chains are in position 1 (△), see *Figure 9*. Right, intercalated side chains are in position 3 (□); the $d = 3.5$ Å reflection is a weaker one

by a separation of clustered side chains equal to 4.49 Å (for non-clustered side chains this distance is 4.77 Å). Side chains that are separated by this distance form a set of lattice planes with a lattice distance of 4.30 Å (angle with the X axis = 53°), see *Figure 9*.

Figure 10b demonstrates the changes in the reciprocal space intensity distribution when intercalated side chains are shifted from position 1 to position 3 (see *Figure 6*). In this way we destroy the ordering characterized by lattice distances of 3.60 and 4.30 Å and generate new sets of lattice planes characterized by lattice distances of 3.50 Å (angle with the Z axis = 15°) and 4.40 Å (angle with the X axis = 23°). In the reciprocal lattice intensity distribution of *Figure 10b* we observe, for example, the extinction of the (002), (202) and (212) reciprocal lattice point intensities (the corresponding lattice distances are 3.60, 4.33 and 4.27 Å, respectively) and the development of high intensity in reciprocal points (102), (112) and (312) (the corresponding lattice distances are 4.37, 4.31 and 3.50 Å, respectively).

The construction of X-ray diagrams follows in the same way as in *Figure 7* for rigid rods. In this way we obtain the schematic pictures of calculated X-ray diagrams shown in *Figure 11*. We see that side chains contribute also to the equatorial reflection at 3.6 Å which is observed only in the perpendicular case. The position 1 reflection at 4.3 Å may be included in the broad meridional streak at 4.5 Å, which spreads on the X-ray diagram of the slowly stretched film (*Figure 5d*) in an angle of 45° from the vertical axis (see also *Figure 19b*). The position 3 reflection at 4.35 Å is included in the 4.2 Å reflection (see *Figure 5b*).

Studying the changes of side-chain ordering, which are represented by a transition of side chains from position 1 to position 3, we have followed the idea that a continuous transition of intercalated side chains between these positions is possible and that, as a consequence, the resulting X-ray picture may be understood as a continuous integration of calculated X-ray diagrams presented in *Figure 11*.

Calculation based on an orthorhombic elementary cell. First, we point out a most interesting connection of the monoclinic cell, equation (3), with the widely

encountered subcell of orthorhombic polyethylene (PE)[6] with the parameters:

$$a = 7.45\ \text{Å};\ b = 4.97\ \text{Å};\ c = 2.54\ \text{Å} \qquad (5)$$

Here the c parameter characterizes the length of a single-plane aliphatic zig-zag chain (*Figure 12*). This structure is in fact almost identical with the structure of clustered side chains, which we obtained as the result of our *ab initio* calculations demonstrated in *Figures 1* and *4*. The closest distance of approach of side chains (interchain separation) in the clustered case was 4.49 Å, while in the crystalline case it was 4.48 Å, hence they are effectively the same. This is a very reliable and important proof of the physical validity of our clustered model. Moreover, comparing the mutual distances between chains in the crystalline and amorphous phases (in *Figure 12*, numbers without and with brackets, respectively), we may suppose that the structure of side chains in the amorphous phase already anticipates, under given preparation conditions, the crystalline structure.

Figure 13 shows an important relation between the reciprocal lattice of the orthorhombic PE single crystal according to equation (5) and the reciprocal lattice constructed for the model of side chains described originally by the monoclinic cell in equation (3). However, in order to reach a more lucid comparison, we describe the model structure of side chains in *Figure 13* by an orthorhombic cell, with the dimensions (according to *Figure 9* and *Figure 2*):

$$A = 10.984\ (5.492)\ \text{Å};\ B = 25.6\ \text{Å};\ C = 7.2\ \text{Å} \qquad (6)$$

In this way we are able to demonstrate the resolution of the experimental X-ray diagram. We see that there is not a great difference between the parts of reciprocal lattices that contribute to the X-ray picture in the perpendicular and/or parallel cases. The changes of the distance between rigid rods (depending on the number n of carbon atoms in the alkyl chain) is expressed in the reciprocal space by the change of the lattice spacing in the c^* (or B^*) direction; however, *Figure 13* demonstrates that the resolution of corresponding scattering features in the perpendicular X-ray diagram is poor. Hence it is not possible to make strict conclusions on the direction of side chains relative to the rigid-rod axis.

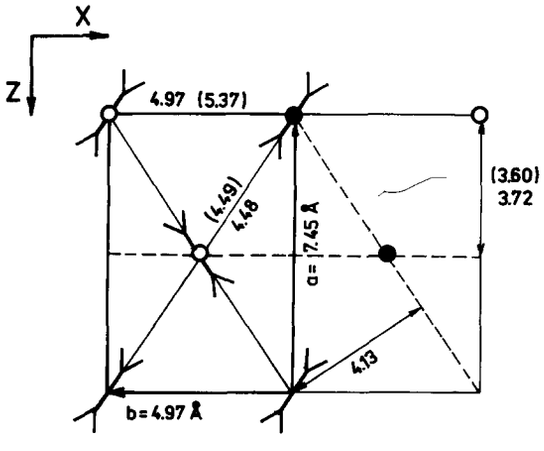

Figure 12 The orthorhombic structure of crystalline polyethylene[6], see equation (5). The c parameter has the value of 2.54 Å. The interchain distance is 4.49 Å and the (110) lattice distance is 4.13 Å. Numbers in brackets indicate interchain distances following from ref. 1

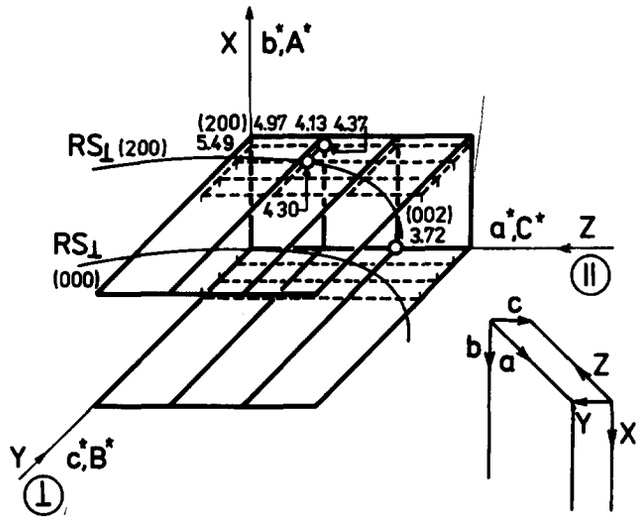

Figure 13 Relation between the reciprocal lattice constructed for the orthorhombic polyethylene (PE) structure according to equation (5) (—) and the orthorhombic reciprocal lattice describing the model of side chains according to equation (6) (– – –). The insert shows the relation between the conventional PE elementary cell axis (*a,b,c*) (*Figure 12*) and the model axis (*X,Y,Z*) used in this paper (*Figures 2* and *9*). Intersections of the reflection spheres with the corresponding reciprocal lattice layer in the perpendicular case are marked $RS_\perp$. Lattice distances are given in Å, e.g. $d(200) = 4.97$ Å corresponds to the PE lattice, while $D(200) = 5.49$ Å corresponds to the model reciprocal lattice

Calculation based on a triclinic elementary cell. It follows from the above paragraph that the preceding model was not able to give a structural interpretation of the 4.5 Å reflection, which is observed in both the perpendicular and parallel X-ray diagrams of all quickly stretched biaxially oriented samples as a meridional reflection and as a broad thick 'meridional' streak spread in an angle of 40° from the vertical axis in the case of slowly stretched samples, see *Figure 5*.

In order to remove this shortcoming we turn our attention to the idea that ordering of side chains may be realized in a similar way to the triclinic structure of PE chains[7]. This structure is described by lattice parameters:

$$a = 4.285\ \text{Å};\ b = 4.825\ \text{Å};\ c = 2.54\ \text{Å};\ \alpha = 90°;\ \beta = 110.25°;$$
$$\gamma = 108° \qquad (7)$$

A schematic projection of this cell into the a,b plane is shown in *Figure 14*.

All observed reflections of cold-worked polyethylene samples, i.e. characterized by $d = 4.56$, 3.80 and 3.55 Å, can then be indexed naturally on a triclinic equatorial network as (010), (100) and (1-10) reflections (see *Figure 15*). The (001) reflection with $d = 2.36$ Å is very weak. All above-mentioned ($hk0$) reflections appear, as expected, as equatorial reflections in X-ray photographs of specimens showing high fibre orientations.

It is important to have a correct orientation of the triclinic PE cell in relation to the coordinate system (X, Y, Z) of the model. This relation is shown schematically in *Figure 14*. Further, there are two possibilities of orientation of the triclinic cell in relation to the stretching direction X of the PPT16 film.

In the first case we suppose that this stretching direction X will be identical with the b-axis of the triclinic cell and that the (100) point ($d = 3.8$ Å) will be precisely in the

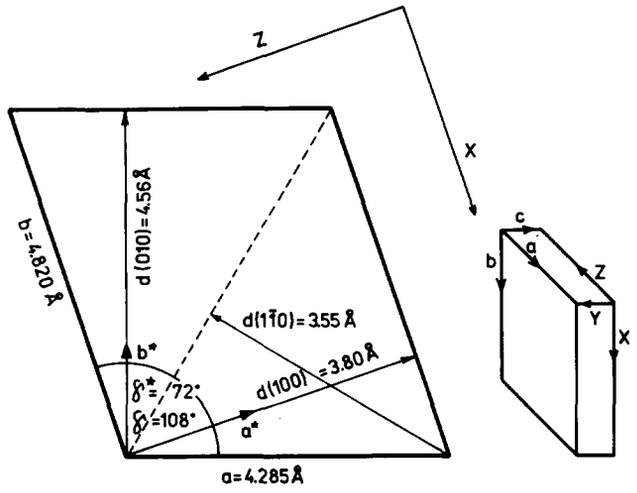

Figure 14 Schematic projection ($\beta = 90°$) of the triclinic polyethylene cell, equation (7), into the a,b plane, showing principal lattice distances and directions of reciprocal lattice vectors a^* and b^*. The orientation of the triclinic a and b axes relative to the x,z coordinates of the PPT16 model used in this paper is important; their mutual orientation is shown in the insert

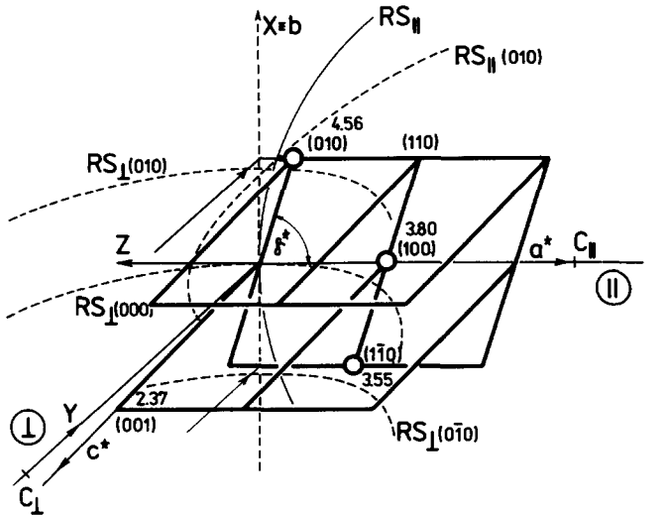

Figure 15 Reciprocal lattice of the triclinic cell proposed for PPT16 in an orientation in which the stretching direction X is identical with the triclinic b axis. This figure demonstrates reflection conditions for the reciprocal lattice points (010), (100) and (1-10). Reflection circles $RS_\perp$ and $RS_\parallel$ are shown; $C_\perp$ and $C_\parallel$ are centres of corresponding reflection spheres. In this orientation the (100) 3.80 Å reflection is equatorial

equatorial position. This situation is visualized in *Figure 15*. The direction of the incident X-ray beam in the parallel case coincides with the a^* axis. The reflection conditions for reciprocal lattice points — (010) 4.55 Å, (100) 3.80 Å and (1-10) 3.55 Å — are easily recognized from the courses of reflection spheres for the parallel and perpendicular directions of the incident X-ray beam. In this orientation of the a^*,b^* plane relative to the incident beam, the 4.5 Å reflection is split at an angle of $\sim 19°$ (the value of the reciprocal angle $\gamma^* \approx 71°$), i.e. it characterizes the experimentally observed broadening. The corresponding calculated X-ray picture shown in *Figure 16* demonstrates, in agreement with experiment, that the 4.55 Å reflection is observed in both cases, while the 3.80 and 3.55 Å reflections are observed only in the perpendicular X-ray diagram.

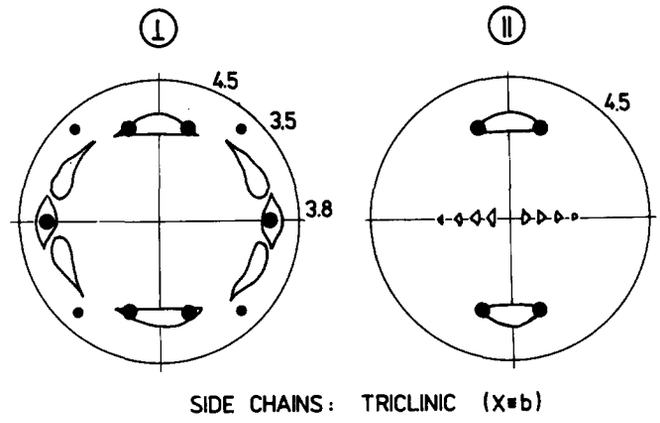

Figure 16 Superposition of the experimental and of the calculated (●) X-ray diagrams for a triclinic structure of side chains in the case when the stretching direction of the PPT16 film is identical with the triclinic b axis. Contours of the experimental X-ray diagrams are shown by thick lines. The $d = 3.5$ Å reflection is weak

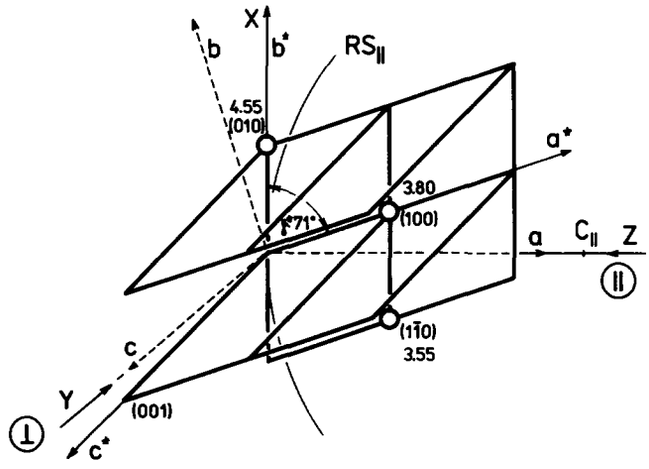

Figure 17 Reciprocal lattice of the triclinic cell proposed for PPT16 in an orientation in which the stretching direction X is identical with the triclinic b^* axis of the reciprocal lattice, i.e. the triclinic a axis is identical with the incident X-ray beam in the parallel case. Conditions for the observation of the 4.5 Å reflection as a meridional one are visualized; $RS_\parallel$ is the reflection sphere (○) and $C_\perp$ its centre in the parallel case. In this orientation of the a^*,b^* plane, the 3.5 Å reflection has the experimentally observed position for the slowly stretched film

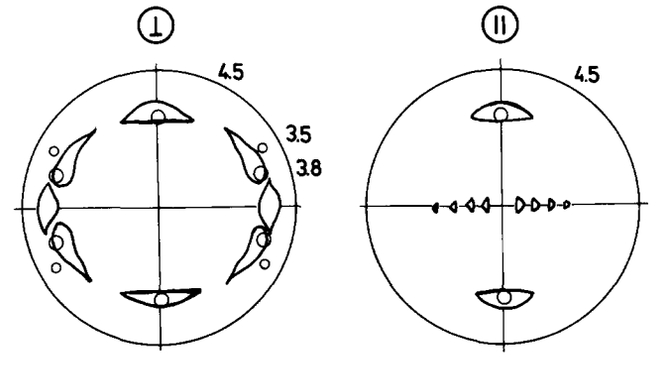

Figure 18 Superposition of the experimental and of the calculated (○) X-ray diagram for an orientation of the triclinic cell in which the incident X-ray beam is in the parallel case identical with the a axis of this cell. Contours of the experimental X-ray diagram are shown by thick lines. The $d = 3.5$ Å reflection is weak

In the second case we suppose that the incident X-ray beam in the parallel case is identical with the *a* axis of the triclinic structure, i.e. it is perpendicular to the *X,Y* layers of the rigid-rod structure. In this orientation the (010) 4.55 Å reflection will be precisely a meridional one. This situation is visualized in *Figure 17* and the corresponding calculated X-ray diagrams are shown in *Figure 18*.

A COMPLEX COMPARISON OF THE CALCULATED AND EXPERIMENTAL X-RAY DIAGRAMS

Figure 19 summarizes the results of our analysis undertaken in the preceding sections for different partial cases. First of all we recognize that the basic contribution to the parallel X-ray diagram comes from the structure of rigid rods described by the orthorhombic cell, equation (2), and from the triclinic structure, equation (7), of side chains.

The analysis of perpendicular X-ray diagrams documents that the structure of side chains is complex and that it

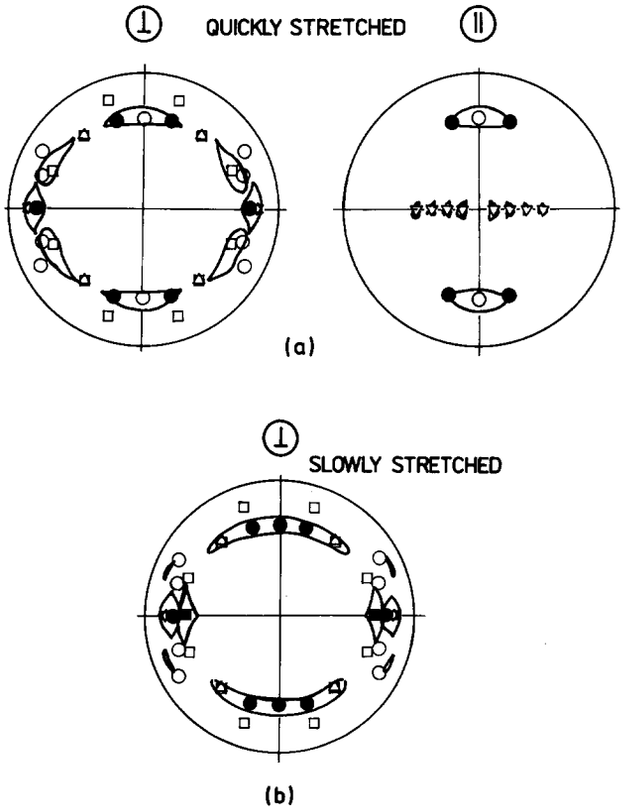

Figure 19 Summary of *Figures 8, 11, 16, 18* and *20*, based on the superposition of the experimental and of the calculated X-ray diagrams for (a) the quickly stretched and (b) the slowly stretched PPT16 film in the perpendicular (⊥) and parallel (∥) cases. The contours of the corresponding experimental X-ray diagrams are shown by thick lines. Symbols: ▽, orthorhombic cell, equation (2), for the model of the rigid rods structure (*Figure 8*); △, monoclinic cell, equation (3), for a model of side chains in position 1 (*Figure 11*); □, monoclinic cell, equation (3), describing a model of side chains in position 3 (*Figure 11*); ●, triclinic cell, equation (7), for a model of side chains in the case when the stretching direction is identical with the triclinic *b* axis (*Figure 16*); ○, triclinic cell, equation (7), for side chains in an orientation in which the triclinic *a* axis is identical with the rigid-rod axis (*Figure 18*); ■, orthorhombic cell, equation (8), for a structure of side chains (*Figure 20*)

can be understood only as a composition of triclinic and monoclinic arrangements. There are two modifications of the monoclinic structure. In the first, all side chains are located on *X, Y* layers defined by the ordering of rigid rods (see the model for position 1, *Figure 9*). This model, however, (see positions marked by triangles in *Figure 19* or *Figure 11*), represents only partial description of the side-chain structure. In the second modification, one half of side chains is diverted out of *X,Y* model layers (see positions 3 in *Figure 9*). This model represents a better partial approximation of the X-ray diagram than the previous one (see square symbols in *Figure 19* or in *Figure 11*). A continuous transition between both models is possible.

In greater part, the side-chain structure is characterized by the triclinic cell, equation (7). This follows from the agreement of calculated positions of reflections for both orientations of this cell in relation to the stretching direction (see open and solid circles in *Figure 19*). The agreement with the experimental X-ray diagram is satisfactory; moreover, it includes the observed broadening of reflections of $\sim 18°$. It is interesting that the weaker 3.5 Å reflection (*Figure 18*) is observed only on the X-ray diagram of the slowly stretched film (see *Figure 19b*).

In the case of the slowly stretched X-ray diagram (*Figure 19b*) there is a very good explanation for the very broad 'meridional' 4.5 Å reflection; however, the equatorial 4.2 Å reflection is not present in any calculated X-ray diagram. It is, however, possible that owing to extreme stretching and preparation conditions[5] an additional deformation of the triclinic cell may occur in the *X,Z* plane, which would make the reciprocal a^* and b^* directions (occupied by reciprocal lattice points characterized by lattice distances $d(100) = 3.80$ Å and $d(010) = 4.56$ Å, see *Figure 14*) mutually perpendicular. This process, marked in *Figure 20* by small double arrows, would then result in an orthorhombic cell O_V described by:

$$A = 9.1 \text{ Å}; \; B = 25.6 \text{ Å}; \; C = 8.4 \text{ Å} \qquad (8)$$

For this cell the calculated intensity (i.e. the calculated value of the structure factor F^2) has for the equatorial (002) reflection a value $F^2_{(002)} = 112\,723$, i.e. it is one of the most intensive of all the above-mentioned structures (e.g. in the monoclinic structure M_3 the analogous structure factor has a value $F^2_{(002)} = 98\,913$). We note also that in the experimental X-ray diagram this reflection is very intense. Hence the proposed ordering characterized by equation (8) represents an important intermediate (transitive) structure enabling the coexistence of other structures typical for the ordering of PE-like chains. *Figure 20* reviews schematically all possibilities discussed in our analysis.

Applying geometrical constructions, similar to those used in *Figures 15* and *17*, to the reciprocal space defined by equation (8), we obtain the positions of the calculated reflections in the calculated X-ray diagram of the slowly stretched film (marked by solid squares in *Figure 19b*). Good agreement is found between the calculated position and the experimental equatorial streak (lattice distance = 4.2 Å). Moreover, there is an overlapping of the calculated meridional position (lattice distance = 4.5 Å) with the calculated one (open circles in *Figure 19*) for the triclinic structure.

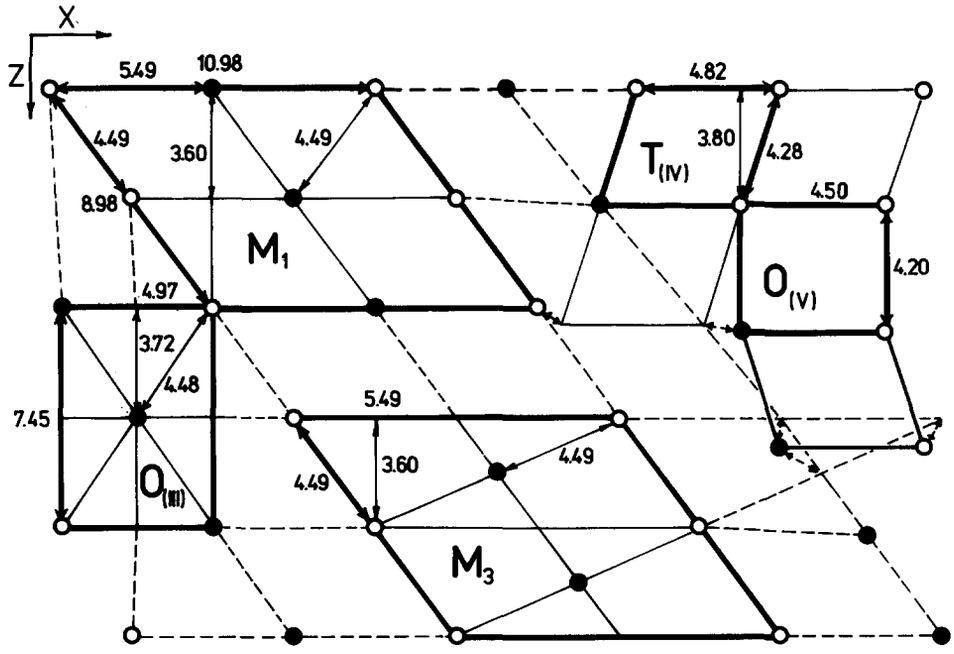

Figure 20 Two-dimensional schematic picture summarizing in the X,Z projection different possible structures of side chains: M_1 and M_3 are monoclinic structures described by equation (4) for intercalated side chains in positions 1 and 3 (see *Figure 9*); O_{III} is the orthorhombic cell of crystalline PE according to equation (5) and *Figure 12*. This cell is shown only to give a better resolution for comparison with other structures; T_{IV} is the triclinic cell (*Figure 14*) drawn similarly as in *Figure 15* in the ($X \equiv b$) position according to equation (7); O_V is the newly proposed orthorhombic structure, equation (8), which is realized only in the case of the slowly stretched film (see *Figure 19b*)

SUMMARY

The basic conclusion following from the analysis of the parallel and perpendicular X-ray diagrams taken on a biaxially oriented polyester, PPT16, is that its overall structure can be characterized as a composition of incommensurate structures: an orthorhombic cell ($A=12.734$ Å; $B=25.6$ Å; $C=7.2$ Å) describes the ordering of rigid rods; the structure of side chains is described by the following cells. (1) By a monoclinic elementary cell ($A=10.984$ Å; $B=25.6$ Å; $C=8.98$ Å; $\beta=126.7°$) which includes two cases. In the first case (M_1) all side chains are in a single layer defined by rigid-rod layers, and in the second case (M_3) (see *Figure 20*) intercalated side chains divert out of these model layers. A continuous transition between both cases is possible. We have shown that this monoclinic cell (which can be easily substituted by an orthorhombic one) differs little from the orthorhombic cell used for the description of the orthorhombic modification of PE, equation (5). Moreover, the arrangement (structure) of clustered side chains, which we found as a result of our *ab initio* model calculations based on the analysis of the amorphous X-ray scattering on a powder sample of this polymer, was almost identical to the crystalline structure of this orthorhombic PE cell. (2) By a triclinic elementary cell T_{IV} ($A=4.820$ Å; $B=25.6$ Å; $C=4.285$ Å; $\alpha=110.25°$; $\beta=108°$; $\gamma=90°$; this description corresponds to a model in the X,Y,Z coordinate system). (3) By an orthorhombic structure O_V ($A=9.0$ Å; $B=25.6$ Å; $C=8.4$ Å) which we found only in the case of the slowly stretched film, and which is a deformation of the above-cited triclinic cell in the X,Z plane.

On the basis of this structural analysis we are also able to understand fully the results of the structural analysis of polyester powder samples which, according to our model calculations[1], include the clustering concept of side chains. In this connection, we return to the question posed in the Introduction, i.e. whether the concept of clustered side chains used for the interpretation of the 'amorphous' structure of side chains in the polyester powder samples (*Figures 1* and *3*) is also able to explain the main features of X-ray diagrams taken on oriented polyesters. It follows from the analysis in the preceding paragraphs that the answer to this question is definitely positive.

In a cluster of side chains, the average interchain distance[1] (between neighbouring side chains) is 4.8 Å, while the average interchain distance (again between neighbouring side chains) resulting as a calculated average distance from all crystalline modifications M_1, M_3, T_{IV}, O_{III}, O_V (shown in *Figure 20*) is also 4.8 Å. This

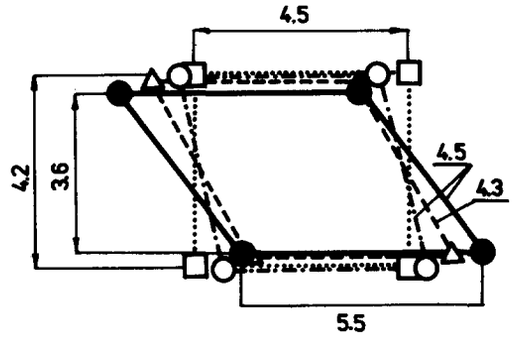

Figure 21 Schematic summary, in the X,Z projection, of the short-range order in different side-chain structures reviewed in *Figure 20*. ——, ●, M_1 structure; –·–·–, ○, M_3 structure; – – –, △, T_{IV} structure; ···, □, O_V structure. The maximal and minimal distances (in Å) in the X and Z directions are given. Underlined numbers denote distances between side chains for the M_1, M_3 and T_{IV} structures

fact documents that the ordering of side chains in the amorphous phase anticipates an interchain distance characteristic of a crystalline arrangement of side chains. However, the long-range order based on the shortest distance is missing; there exists only the medium-range ordering characterized in our model calculations for powder samples by the monoclinic cell, equation (4).

In *Figure 21* we present the result of a more profound inspection of interchain distances and cell dimensions occurring in different structures visualized in *Figure 20*. This analysis shows that the short-range order of side chains in the monoclinic M_1 and M_3 structures (i.e. the short-range order of side chains proposed originally for the amorphous structure) differs only a little from the short-range order of side chains in, for example, the triclinic T_{IV} and/or orthorhombic O_V structures. This is the main reason why models based on cells M_1 and M_3, in the case of polyester powder samples, enable not only the success of model calculations interpreting the 'amorphous' X-ray scattering by the Debye equation[1] but also the good result of the X-ray scattering calculations based on the 'crystalline approach', demonstrated in *Figure 4*.

ACKNOWLEDGEMENT

Thanks are due to Professor G. Wegner (Max Planck Institute for Polymer Research, Mainz) for allowing use of the experimental results of the dissertation by A. Zens. Special thanks are due to Dr J. Baldrian (Institute of Macromolecular Chemistry, Academy of Sciences of the Czech Republic) for valuable discussions concerning the interpretation of X-ray diagrams of oriented polymers. Discussions with Professor M. Ballauff (Institute for Polymer Research of the University of Karlsruhe) are greatly appreciated. Professor E. W. Fischer (Max Planck Institute for Polymer Research, Mainz) is also thanked for his kind support in enabling this paper to be published.

REFERENCES

1 Červinka, L. and Ballauff, M. *J. Colloid Polym. Sci.* 1992, **270**, 859
2 Ballauff, M. and Schmidt, G. F. *Mol. Cryst. Liq. Cryst.* 1987, **147**, 163
3 Červinka, L. *J. Non-Crystalline Solids* 1988, **106**, 291
4 Červinka, L., Fischer, E. W., Hahn, K., Jiang, B. Z., Hellmann, G. P. and Kuhn, K. Z. *Polymer* 1987, **28**, 1287
5 Zens, A. Thesis, Johannes Gutenberg Universität, Mainz, 1989
6 Tadokoro, H. in 'The Structure of Crystalline Polymers', Wiley, 1979, p. 51
7 Turner-Jones, A. J. *Polym. Sci.* 1962, **62**, 553